crystals

MDPI

Article

Splitting Opaque, Brittle Materials with Dual-Sided Thermal Stress Using Thermal-Controlled Fracture Method by Microwave

Xiaoliang Cheng [1,*], Zongyang He [2], Hailong Wang [2] and Yang Wang [2]

[1] School of Mechanical Engineering, Anhui Polytechnic University, Wuhu 241000, China
[2] School of Mechatronics Engineering, Harbin Institute of Technology, Harbin 150001, China; hit_hezongyang@126.com (Z.H.); whl19850505@163.com (H.W.); yangwanghit@163.com (Y.W.)
* Correspondence: chengxiaoliang@ahpu.edu.cn

Abstract: The thermal-controlled fracture method has been increasingly focused upon in the high-quality splitting of advanced brittle materials due to its excellent characteristics related to the fact that it does not remove material. For opaque, brittle materials, their poor fracture quality and low machining capacity resulting from their single-sided heat mode is a bottleneck problem at present. This work proposed the use of dual-sided thermal stress induced by microwave to split opaque, brittle materials. The experimental results indicate that the machining capacity of this method is more than twice that of the single-sided heat mode, and the fracture quality in splitting opaque, brittle materials was significantly improved by dual-sided thermal stress. A microwave cutting experiment was carried out to investigate the distribution characteristic of fracture quality by using different workpiece thicknesses and processing parameters. A dual-sided thermal stress cutting model was established to calculate the temperature field and thermal stress field and was used to simulate the crack propagation behaviors. The accuracy of the simulation model was verified using temperature measurement experiments. The improvement mechanism of the machining capacity and fracture quality of this method was revealed using the fracture mechanics theory based on calculation results from a simulation. This study provides an innovative and feasible method for cutting opaque, brittle materials with promising fracture quality and machining capacity for industrial application.

Keywords: opaque; brittle materials; thermal-controlled fracture method; dual-sided thermal stress; microwave cutting; machining capacity; fracture quality; simulation model; crack propagation behavior

Citation: Cheng, X.; He, Z.; Wang, H.; Wang, Y. Splitting Opaque, Brittle Materials with Dual-Sided Thermal Stress Using Thermal-Controlled Fracture Method by Microwave. *Crystals* **2022**, *12*, 801. https://doi.org/10.3390/cryst12060801

Academic Editor: Umberto Prisco

Received: 11 May 2022
Accepted: 30 May 2022
Published: 6 June 2022

1. Introduction

Opaque, brittle materials, mainly including advanced ceramics, have been widely used in industrial fields due to their excellent properties of high-temperature performance, low expansion, high hardness and corrosion resistance. However, these intrinsic characteristics induce processing difficulties, especially in the splitting process of separating a whole blank into small pieces. The conventional cutting method depends on removing surplus materials between the parts by contact force, melting, ablation, etc. Due to its brittleness, these methods tend to damage fresh surfaces and cause serious fracture quality problems such as micro-cracks, stripes and heat-affected zones [1].

In 1968, Lumley proposed the method of guiding crack propagation by thermal stress to split brittle material. According to its processing principle, it is called the thermal-controlled fracture method (TCFM) [2]. The TCFM has the advantages of no material removal, no high temperature effect (under 500 °C) and no force impact. It can achieve high splitting efficiency (its splitting speed can reach more than 10 mm/s) and good fracture quality (its arithmetic mean deviation of contour (Ra) can reach less than 10 nm) [3]. Therefore, the TCFM has obvious advantages compared with conventional cutting techniques such as abrasive wheel cutting, diamond saw cutting, abrasive water jet machining, ultrashort pulse laser beam ablation methods and other processing method [1,4–7], and has become a promising machining method, attracting the interest of many researchers in the field of brittle material processing [8–12]. The thermal stress used to split material in the TCFM is produced by a heat source on the surface or in the body of the workpiece (as shown in Figure 1).

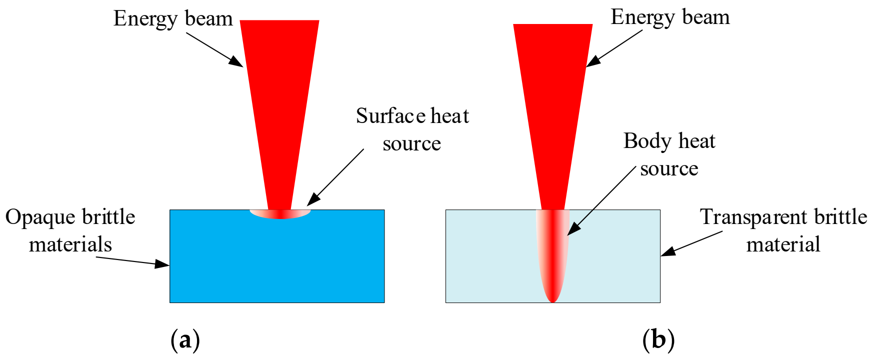

Figure 1. Schematic diagram of heat source type in thermal-controlled fracture method. (**a**) Surface heat source, (**b**) body heat source.

The site of a heat source in a material is mainly determined by its absorption type for energy sources such as laser beam. The research regarding splitting glass using the TCFM have proven that the body absorption type which produces body heat sources can produce better processing quality than that of surface heat sources [3,9]. Using body heat sources, the process of splitting LED glass using the TCFM has been realized in industrialization [13]. However, a body heat source is mainly formed in transparent, brittle materials such as glass. For opaque, brittle materials, a thermogenic beam such as a laser beam can only be absorbed by the surface of the material to form a surface heat source [14–17]. Since the heat source is formed on a single surface of the material in these cases, this cutting mode is called the single-sided thermal stress method (SSTM).

The SSTM is mainly used for cutting thin brittle materials such as silicon wafer, sapphire and ceramic substrate (generally no more than 1 mm thickness). Ueda used the SSTM to cut silicon wafers and ceramic sheets, and the results indicated that the surface roughness can reach 100 μm for Si_3N_4, 1.3 μm for Al_2O_3 ceramic and 0.7 μm for crystalline silicon; however, the thickness of these specimens was only 0.5 mm [8]. Although it has ideal processing quality for thin materials, it has been reported that the cutting quality by the single-sided cutting mode is remarkably worse than that of the full-body cutting form for thick brittle materials [13,17]. The work of Saman indicated that the worse fracture quality by the SSTM is because the effect of thermal stress on thickness is not adequate for the material to be cut, and its maximum tensile stress is in the reverse side of the pre-crack [18]. Cai used a laser to cut thick Al_2O_3 ceramic materials, and the results indicated that it was difficult to split thick ceramic materials with the single-sided heat mode, and its processing quality was poor [19]. Thus, the machining capacity and processing quality of the SSTM hinder the application of the TCFM in the field of cutting opaque, brittle materials.

Due to the high dielectric properties, some opaque, brittle materials have good absorption capacity for microwaves. This means these ceramics can form body heat sources via microwave beams. Wang successfully used a microwave of 2.45 GHz to treat SiC ceramics in the full-body cutting form using the TCFM [20]. However, for those other opaque, brittle materials such as Al_2O_3 and Si_3N_4 ceramics, which have low dielectric coefficients, heating in the body form via microwave is as difficult as it is with laser beams. Cheng and Wang used microwaves to cut Al_2O_3 ceramics coated with graphite, which has good absorptivity for microwaves; this method is an SSTM [21,22].

To overcome the defects of the SSTM, Cai used dual laser beams to cut glass–silicon–glass plates based on the TCFM [23]. However, the dual laser beams method requires relatively complex alignment technology, and the two laser beams need to have exactly the same operation states, which results in a great increase in processing costs. Furthermore, the minimum temperature needed to split brittle material using laser beams in the TCFM is higher than that needed for microwaves, which would induce unnecessary thermal damage [20].

In this work, microwave-induced dual-sided thermal stress (MIDT) was proposed for splitting opaque, brittle materials to improve the machining capacity and processing quality of the SSTM. Compared with the dual laser beams method, MIDT needs just one energy source. The high dielectric loss material of graphite was used to coat the upper and lower surfaces of the processing area of the opaque, brittle plates to form a dual heat source. The microwave absorbed by the upper surface was used to form an upper heat source, and the remainder of the energy penetrating the ceramic plate was absorbed by the lower surface and used to form lower heat source. Cutting experiments were conducted to study the machining capacity and the effects of processing parameters on fracture quality. An MIDT cutting simulation model was developed to analyze the improvement mechanism of the machining capacity and fracture quality using this method. This method demonstrated significant potential for the precise cutting of thick opaque, brittle materials using the thermal-controlled fracture method.

2. Experiment

2.1. Experimental Principle

Al_2O_3 ceramic is an opaque, brittle material that has a low dielectric coefficient. The cutting of this ceramic with the TCFM is usually performed in the single-sided heat mode. Figure 2 shows the schematic diagram of heating low-dielectric-coefficient materials on their dual-sided surface via microwaves. In this work, high-dielectric-coefficient graphite material was used to coat the upper and lower surfaces of the low-dielectric-coefficient Al_2O_3 ceramics to absorb microwaves and generate upper and lower surface heat sources. To control the distribution of the heat sources, the coating material was restricted within a certain range along the cutting line.

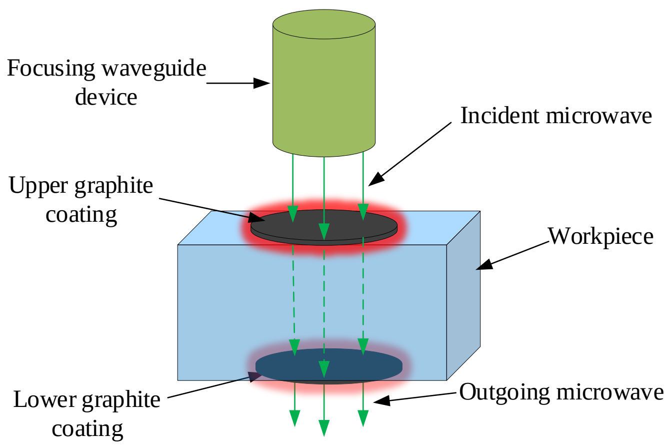

Figure 2. Schematic diagram of single microwave beam heating upper and lower surface of the material.

The cutting of ceramic via MIDT was realized by the heat generated by high electromagnetic loss on the dual side of the coating material to induce thermal stress and guide crack propagation. It is feasible to use one waveguide output to realize dual-sided thermal stress because only part of the energy was lost when the microwave irradiated the upper coating materials. The remaining microwave energy could pass through the dielectric ceramic without much electromagnetic loss onto the lower surface coating material to generate heat. In this way, the upper and lower coating materials directly transferred the heat generated by electromagnetic loss to the workpiece and produced dual-sided thermal stress. Since the upper and lower heat sources were generated by the same microwave beam, the neutrality of the heat source did not need to be adjusted. Compared with the dual laser beam heating scheme adopted by Zhao and Cai, this project greatly reduces the equipment and technical costs [9,10,23].

A schematic diagram of cutting ceramic via MIDT is shown in Figure 3. As is shown, the heat sites in both sides were located directly below the waveguide output (Figure 3a). The uneven heat distribution produced a thermal stress field in the material. The tip of prefabricated crack could produce a stress amplification effect and was the weakest position at the same time. When the tensile stress at the tip exceeded the fracture limit of the material, the crack system reached the cracking condition. Based on the appropriate moving speed between the material and the waveguide generated by the motion device, the crack propagated forward at the appropriate speed, so as to realize the cutting of the material (Figure 3b,c). Since the thermal stress was induced at the dual side of the material at the same time, this is called the microwave-induced dual-sided thermal stress cutting method.

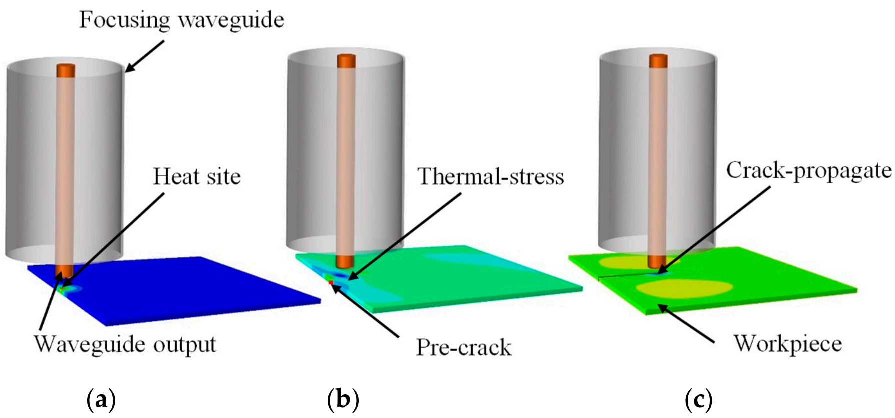

Figure 3. Schematic diagram of cutting ceramic by using microwave-induced dual-sided thermal stress. (**a**) Heating stage; (**b**) thermal stress stage; (**c**) crack propagation stage.

2.2. Experimental Material and Apparatus

Figure 4 shows the schematic diagram of the microwave-induced dual-sided thermal stress cutting system and the cutting machine. The microwave generated by the microwave source was modulated by the Bj26 waveguide device and was guided into the focusing equipment. Then, the focusing equipment output focused the microwave for processing from the inner conductor. The workpiece with a highly dielectric coating was directly below the inner core of the waveguide output. In order to obtain the accurate cutting position and movement, the workpiece was placed on an NC motion device which could realize x-y-z three-direction movement. The function of the z-axis was to adjust the distance between the inner core of the waveguide and the workpiece to achieve specific power density. The microwave cutting machine tool was equipped with safety facilities such as a safety filter screen, microwave absorption vessel and microwave safety door to ensure safety and reliability. The microwave frequency used in this study was 2.45GHz, and the maximum output power of the equipment was 1500 W.

Figure 5 shows the workpiece of Al_2O_3 ceramic, in which the black part in the middle is the coated graphite which had a thickness of 0.1 mm and a width of 1 mm. The dimensions of the ceramic material were 100 mm $\times$ 100 mm in size, and the thickness had different specifications of 1 mm, 2 mm, 4 mm, 6 mm and 8 mm. The coating position was symmetrically distributed on the upper and lower surfaces along the cutting line. A pre-crack was fabricated on the end of the workpiece with a diamond wire saw. The graphite was a micron-sized powder material (mesh of 8000 and particle size of 1.6 μm), evenly prepared with alcohol and then coated onto the surface of workpiece with precision powder spreading equipment.

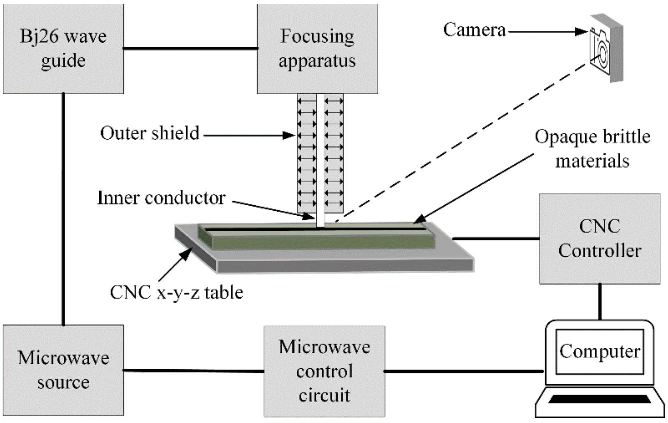

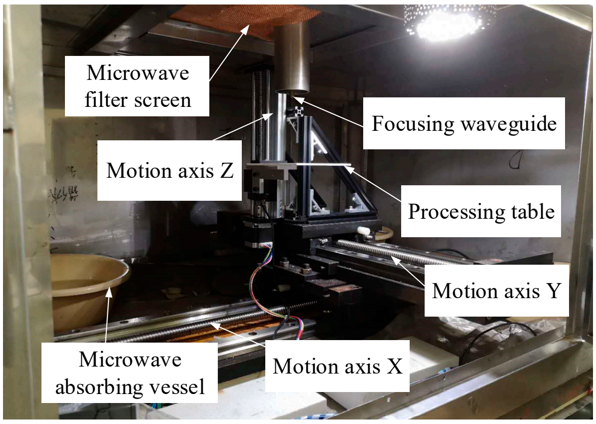

Figure 4. The microwave-induced dual-sided thermal stress cutting machine. (**a**) Schematic of the experimental apparatus; (**b**) microwave-induced dual-sided thermal stress cutting machine.

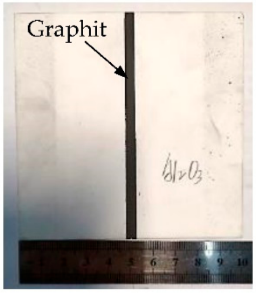

Figure 5. Al_2O_3 ceramic plate coated with graphite.

Table 1 shows the range of processing parameters used in the experiment. The main processing parameters which could be controlled were microwave power and scanning speed.

Table 1. Processing parameters of in microwave cutting of Al_2O_3 ceramic using TCFM.

Test Group No	Workpiece Thickness (mm)	Single-Sided Heat Source		Dual-Sided Heat Source	
		Microwave Power (W)	Scanning Speed (mm/s)	Microwave Power (W)	Microwave Power (W)
NO.1	1	600–1200	2.0–3.5	400–700	2.0–3.5
NO.2	2	900–1500	0.5–2.0	800–1100	2.0–3.5
NO.3	4	1200–1500	0.3–0.6	1200–1500	1.0–2.5
NO.4	6	1200–1500	0.1–0.4	1200–1500	0.5–2.0
NO.5	8	1200–1500	0.1–0.4	1200–1500	0.25–1.00

In order to study the effect of dual-sided heating method on the machining ability, experiments with both single-sided and dual-sided heat sources for cutting ceramic using TCFM were carried out. Each test was repeated four times. The mean values were selected as the final results. These processing parameter ranges were determined in advance by a thermal stress cutting simulation. The guidance for determining the processing parameter range from the simulation was that the cutting process could be realized and had acceptable crack propagation quality. To investigate the distribution characteristics of the fracture quality via MIDT, the surface roughness of the fracture surface was measured at 10 mm, 50 mm and 90 mm along the cutting direction, with three measurement positions along the thickness direction at each site. The distribution of these measurement sites is shown in Figure 6.

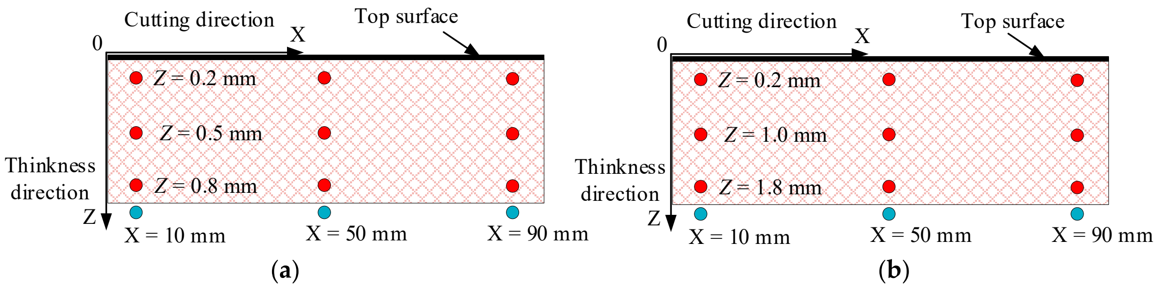

Figure 6. Location of surface roughness measurement points in fracture surface of the workpiece with different thickness of material. (**a**) 1 mm; (**b**) 2 mm.

3. Results

3.1. Machining Capacity

Table 2 shows the experimental results of machining capacity in the cutting of Al_2O_3 ceramic by using the TCFM induced by single-sided and dual-sided heat sources. The processing parameters shown in Table 1 could realize the cutting of ceramic materials and achieve acceptable cutting quality at the same time. It can be seen from Table 2 that when the single-sided heating method was adopted, the maximum processing thickness was 2 mm, while the dual-sided heat source could realize 8 mm. It is notable that the cutting speed could be more than 100 times higher than that of the diamond wire saw cutting method, which was about 0.01 mm/s [24].

Table 2. Experimental results of machining capacity in cutting of Al_2O_3 ceramic by using TCFM.

Workpiece Thickness (mm)	Single-Sided Heat Source		Dual-Sided Heat Source	
	Microwave Power (W)	Cutting Speed (mm/s)	Microwave Power (W)	Cutting Speed (mm/s)
1	1000	3	600	3
2	1500	0.5/1.0	1000	3
4	——	——	1500	2
6	——	——	1500	1
8	——	——	1500	0.5

Figure 7 shows the experimental results of cutting Al_2O_3 ceramic with thickness of 8 mm with MIDT. They indicate that the MIDT cutting method can achieve an excellent fracture surface and an approximately straight crack propagation path.

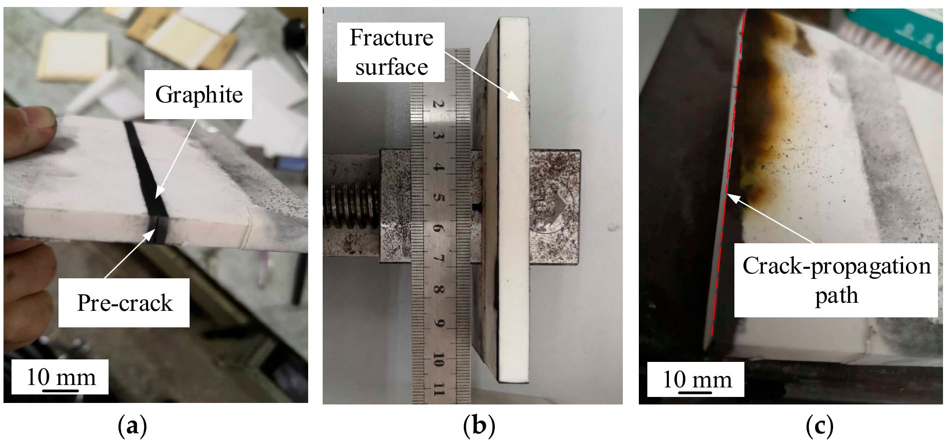

Figure 7. Experimental results of cutting Al_2O_3 ceramic with thickness of 8 mm with MIDT. (**a**) The workpiece before cutting, (**b**) fracture surface after cutting, (**c**) top surface and the crack propagation path after cutting.

3.2. Fracture Quality

Figure 8 shows the fracture surface micrograph and 3D outline figure of the workpiece after cutting Al_2O_3 ceramic materials with thicknesses of 2 mm and 8 mm by using MIDT. The sampling location of the 8 mm thickness was at the middle depth of the material with the same scale of the 2 mm thickness. The processing parameters for these two thicknesses of ceramic materials are shown in Table 1. From Figure 8b, it can be seen that most areas in the middle depth were relatively flat and were much better than those near the surface. At the middle depth of 8 mm thickness, the contour fluctuation was greater than that of the material with 2 mm thickness with larger irregularity. The arithmetic average surface roughness Ra at the middle depth after cutting could achieve 4 μm when cutting the workpiece with 8 mm thickness. This was much better than that of the wire saw cutting method, which is the most popular technique used to cut ceramics [1].

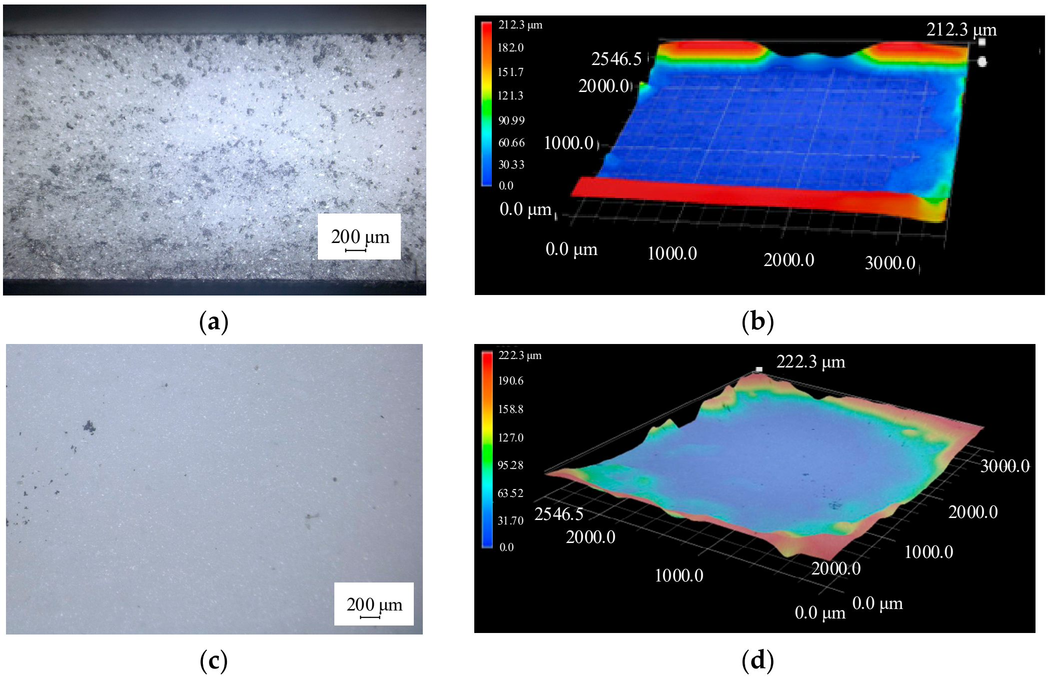

Figure 8. Fracture surface in cutting Al_2O_3 ceramic using MIDT. (**a**) The micrograph of fracture surface with thickness of 2 mm, (**b**) 3D figure of fracture surface of material with thickness of 2 mm, (**c**) the micrograph of fracture surface with thickness of 8 mm, (**d**) 3D figure of fracture surface of material with thickness of 8 mm.

Figure 9 shows a 3D figure of the section profile of Al_2O_3 ceramic with a thickness of 2 mm cut with a microwave-induced single-sided heat source using the TCFM. The processing parameters used are shown in Table 1, where the cutting speed used was 1.0 mm/s. Comparing Figures 8 and 9, it is notable that dual-sided induced thermal stress could obtain better fracture quality than that of single-sided induced thermal stress.

Figure 10 shows the effect of microwave power on surface roughness Ra in cutting Al_2O_3 ceramics using MIDT. It can be seen that the fracture quality of the material 1 mm thickness was better than that with 2 mm thickness. The surface roughness Ra increased dramatically with the increase in microwave power, which was independent of material thickness. It is noteworthy that the fracture quality in the middle section was much better than that in the inlet and outlet of the material. The fracture quality in the middle section, shown in Figure 10c,d, indicated that the fracture quality at the middle depth is better than that near the surface. The fracture quality shown in Figure 10c was better than that achieved with the laser-induced single-sided thermal stress method reported by [8], in which the Ra was 1.3 μm and the thickness was 0.5 mm, which was thinner than that in this study.

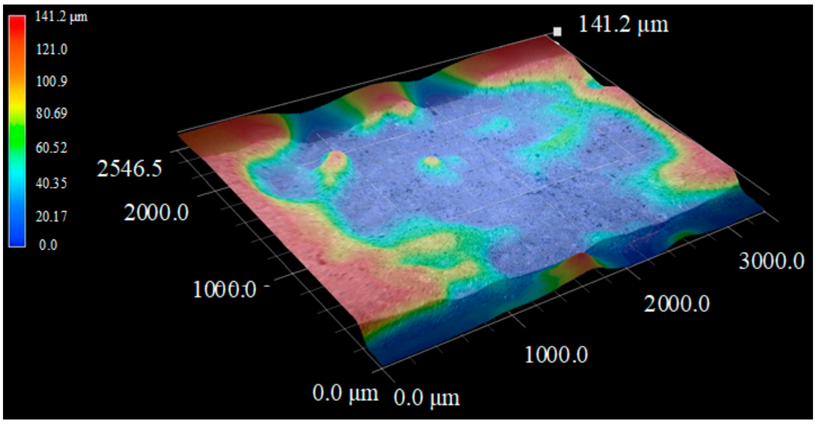

Figure 9. Fracture surface of Al_2O_3 ceramic with thickness of 2 mm cut with microwave-induced single side surface heat source.

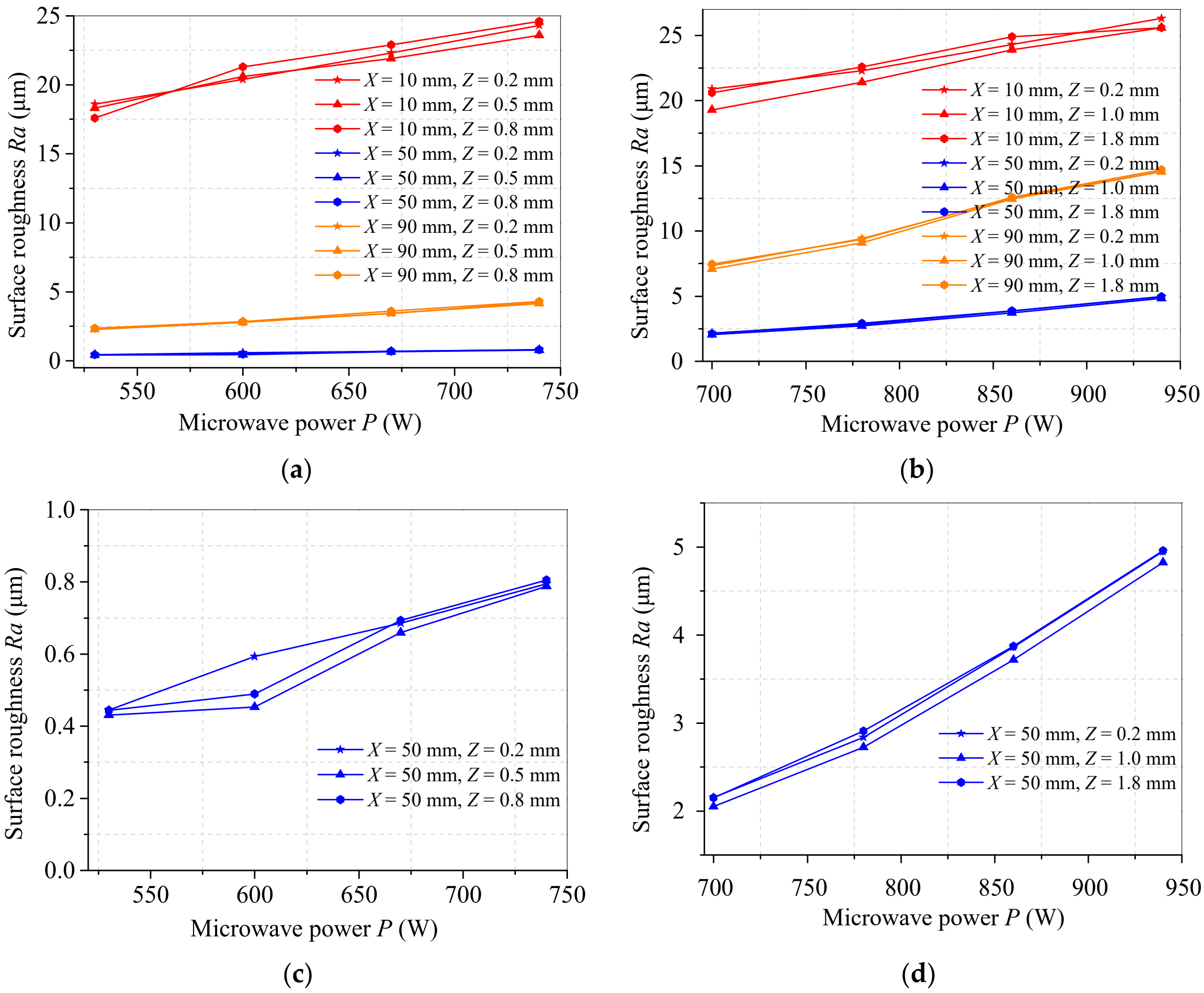

Figure 10. The influence of microwave power on the surface roughness Ra of fracture surface in cutting Al_2O_3 ceramic using MIDT. (**a**) Fracture quality along the cutting direction with thickness of 1 mm, (**b**) fracture quality along the cutting direction with thickness of 2 mm, (**c**) fracture quality distribution along thickness at the middle section with thickness of 1 mm, (**d**) fracture quality distribution along thickness at the middle section with thickness of 2 mm.

4. Discussion

4.1. Finite Element Modeling of the Cutting Process

The main physical processes of cutting opaque, brittle materials with MIDT are as follows:

(1) Absorption of microwave and heat generation.

The microwave is absorbed at the upper coating material, and then it penetrates the ceramic material body almost without loss and is absorbed by the lower coating material. In this way, the microwave is absorbed by the upper and lower coating materials and dual-sided surface heat is generated. The thermal power density on the upper and lower surface can be calculated by

$$P_Z = 2\pi f \varepsilon_0 \varepsilon_r \tan\delta |E_t(x, y, z)|^2 \tag{1}$$

where P_Z (W/m^3) is the thermal power density, f (GHz) is the microwave frequency, ε_0 (8.85×10^{-12} F/m) is the vacuum permittivity, ε_r is the relative permittivity of graphite, δ is dielectric loss angle and $E_t(x, y, z)$ (V/m) is the electric field intensity.

(2) Heat transfer process.

The heat generated at the upper and lower surfaces is transmitted from the surface to the ceramic material body. This process is accompanied by changes in heat convection and heat radiation between the material and the environment.

According to Fourier heat transfer and energy conservation law, taking the plane where the surface heat source is located as the X-Y plane and the direction which is perpendicular to the plane as the Z axis in the Cartesian coordinate system, the heat transfer differential equation inside the workpiece in a non-equilibrium state can be expressed as

$$\rho c \frac{\partial T}{\partial t} = \frac{\partial}{\partial x}\left(\lambda \frac{\partial T}{\partial x}\right) + \frac{\partial}{\partial y}\left(\lambda \frac{\partial T}{\partial y}\right) + \frac{\partial}{\partial z}\left(\lambda \frac{\partial T}{\partial z}\right) + \dot{Q}(x,\ y,\ z,\ t) \tag{2}$$

where ρ is material density (Kg·m^{-3}), c is specific heat (J/Kg·°C), λ is thermal conductivity (W/m·°C) and $\dot{Q}$ is heat production per unit volume (J·m^{-3}), which is related to P_Z in Equation (1). The heat convection and the heat radiation between the workpiece and the environment also needs to be considered.

(3) Thermal stress generation.

According to the thermal stress theory, the uneven heat distribution induces thermal stress in the material. The calculation of a thermal stress field is mainly based on the following constitutive equation:

$$\sigma_{ij} = D_{ijmn}\varepsilon_{mn} - \beta_{ij}T \tag{3}$$

where σ_{ij} is the stress component (MPa), D_{ijmn} is the elastic coefficient (MPa), ε_{ij} is the strain component, T is the temperature distribution in Equation (3) and β_{ij} is the thermal stress coefficient (MPa). The solution of thermal stress needs to combine geometric equations and equilibrium differential equations.

(4) Crack propagation process.

When the tensile stress acts on the prefabricated crack and exceeds the fracture strength of the material, the pre-crack can propagate. This process includes the mutual transformation of elastic energy and surface energy in the crack system.

When the vertical tensile stress component of the crack tip σ_A is greater than the critical stress σ_F, the crack begins to propagate, and the material begins to be cut. σ_F can be expressed as

$$\sigma_F = \left[2E'\gamma/(\pi c_0)\right]^{1/2} \tag{4}$$

where c_0 is the size of the pre-crack (m), E' is the equivalent elastic modulus (Pa) and γ is free surface energy per unit area (J/m^2). σ_A can be obtained by Equation (3) using the finite element method (FEM).

The cutting of opaque, brittle materials via thermal stress is an uncoupled thermoelastic physical process, in which the calculation of the temperature field, thermal stress field and crack propagation requires finite element modeling (FEM) technology. Based on the above theoretical modeling, the calculation of the temperature field, stress field and crack propagation in cutting opaque, brittle materials via MIDT was realized by using the finite element simulation software ABAQUS. The mechanical and thermophysical properties of Al_2O_3 ceramic materials are shown in Table 3.

Table 3. Mechanical and thermophysical properties of Al_2O_3 ceramic.

Physical Parameters	Value
Thermal conductivity (W/m·°C)	25
Density (g/cm^3)	3.9
Specific heat (J/Kg·°C)	880
Expansion coefficient (10^{-6}/°C)	7.5
Young's modulus (G Pa)	370
Poisson ratio	0.22

Figure 11 shows the workpiece mesh model used in the simulation. The geometric dimension of the model was 100 mm × 100 mm × 1 mm. Due to the large size of the workpiece, the balance between calculation accuracy and calculation efficiency needed to be considered. Therefore, mesh refinement was carried out around the crack propagation zone, and coarse mesh was used in the other sites. The refinement of the middle part, which had a 10 mm width, was the scanning mesh type, and the coarse mesh at other positions was of the structured mesh type. The minimum mesh size was 0.071 mm and was along the thickness direction of the workpiece.

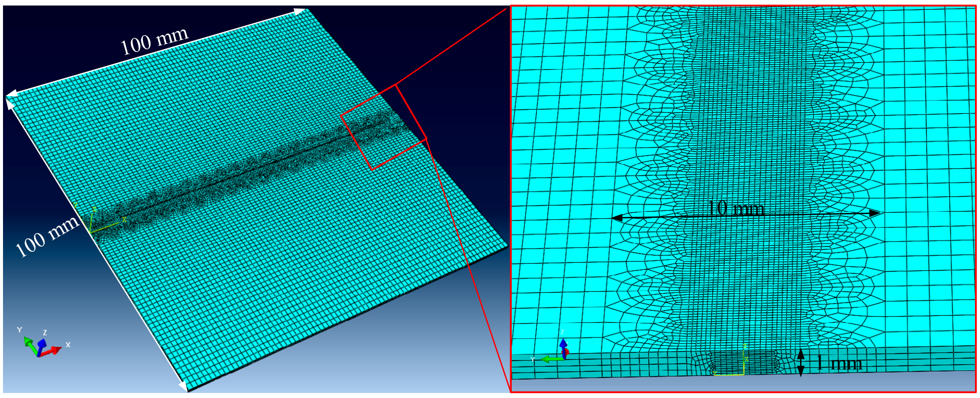

Figure 11. Workpiece mesh model.

Figure 12 shows the finite element simulation flow. The reasonable construction and setting were mainly carried out from three aspects: geometric modeling, physical modeling and the calculation method. The temperature was the loading condition for subsequent thermal stress and crack propagation simulation. The accuracy of the calculation results was related to the reliability of the whole model.

Thus, the simulated temperature needed to be verified by experiments to check the accuracy of the model. The optical fiber temperature measurement experiment was carried out to verify the temperature simulation results. Figure 13 shows the comparation between the temperament measurements results and the prediction results from the simulation. From Figure 13, it can be seen that the simulation results had good agreement with the experimental results. This indicates that the model was established correctly and could be used to analyze the cutting mechanism in this process.

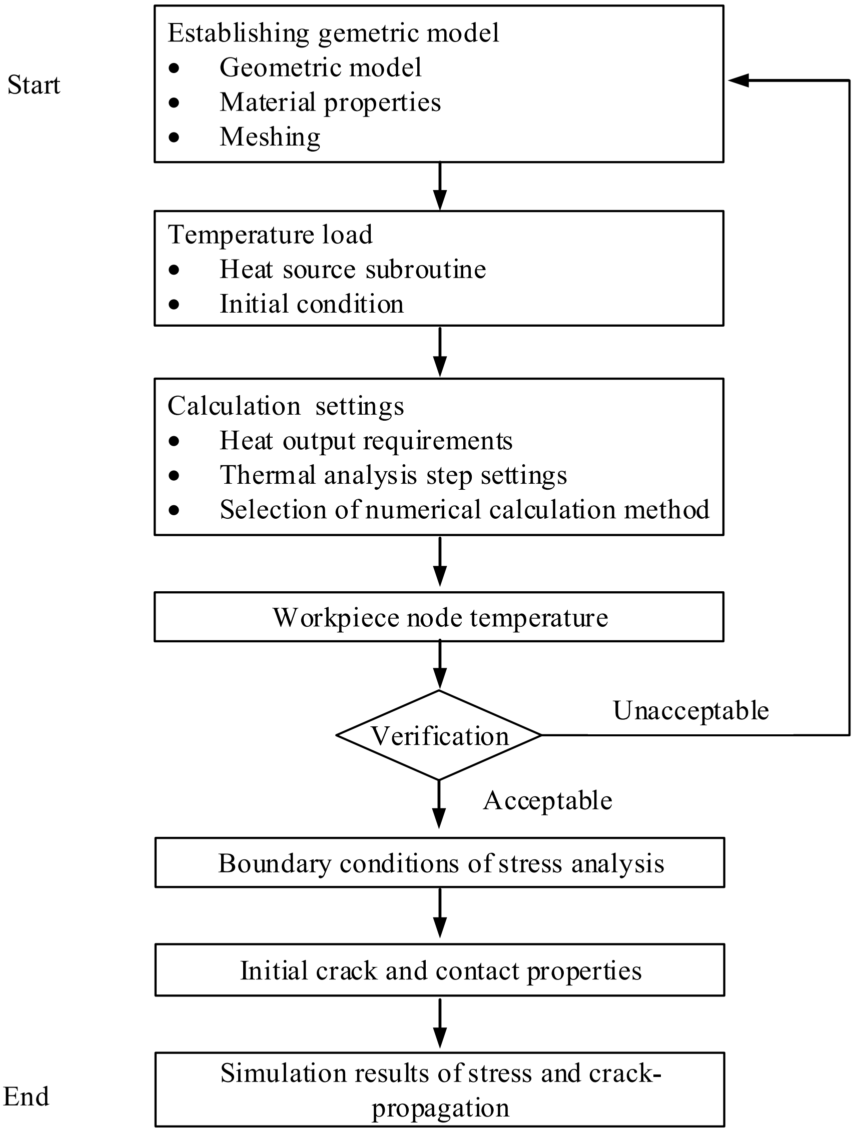

Figure 12. Flow chart of simulation process.

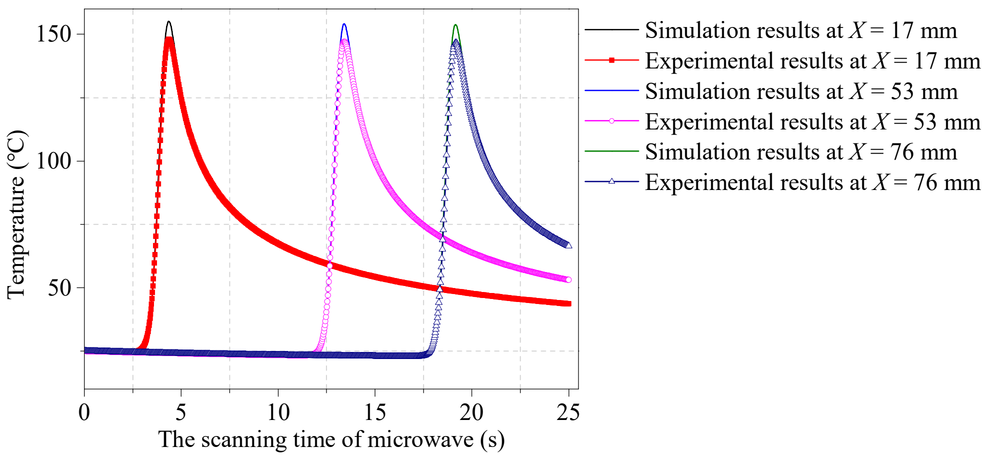

Figure 13. Comparation between the temperature simulation results and the experimental results.

4.2. Mechanism of the High Machining Capacity

Figure 14 shows the evolution of the temperature field induced by the dual-sided heat method. The scanning speed of the heat source was 3 mm/s, the microwave power was 600 W, the thickness of the workpiece was 1 mm and the dimensions of the other two directions were 100 mm. From Figure 14, it can be seen that the upper and lower heat-affected zone induced by the two heat sources kept approaching and finally connected as a thin waist shape. It can be derived that the deeper heating zone (at least twice as much) produced by the dual-sided heat mode was a direct reason for the improvement in the machining capacity. The effective heating depth enhanced by the dual-sided heat mode was more than twice that of the single-sided heat mode, because there was no low-temperature convection in the case of the dual-sided heating mode. This is the reason why the machining capacity of the dual-sided heating method was more than twice that of the single-sided heating method.

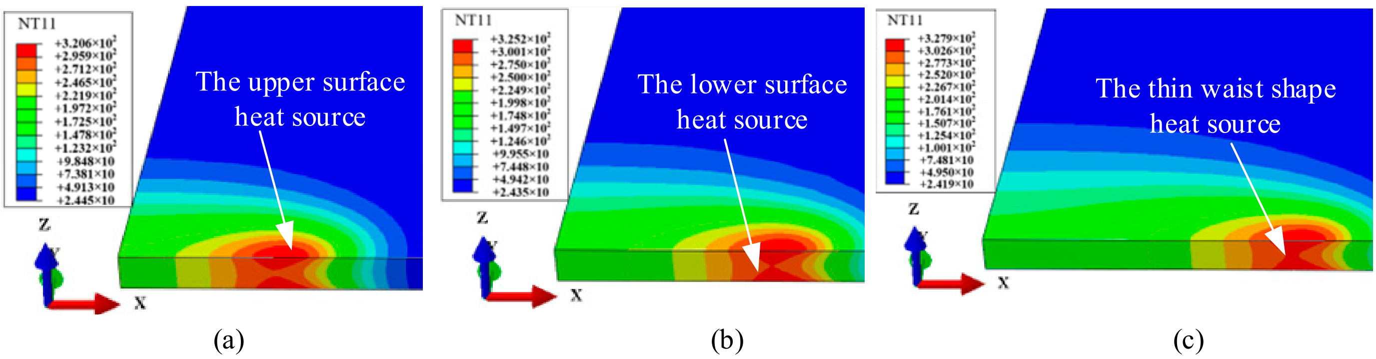

Figure 14. Evolution of temperature field in cutting Al_2O_3 ceramics with dual-sided heat mode at (**a**) 2.433 s, (**b**) 3.033 s and (**c**) 4.033 s.

Figure 15 shows the evolution of the transverse tensile stress induced by the dual-sided heat method. From Figure 15, it can be seen that the maximum compressive stress was divided into upper and lower areas at first and then kept approaching and connected as a thin waist shape. It could be found that the tensile stress zone in front of the compressive stress zone, which was used to cut the workpiece, had an integrated shape. Figure 16 shows the contrast of the distribution of the thermal stress of the single and dual-sided heat modes and their effect on the on the maximum cutting thickness. It is notable that the depth of the tensile stress had a positive correlation with the machining capacity.

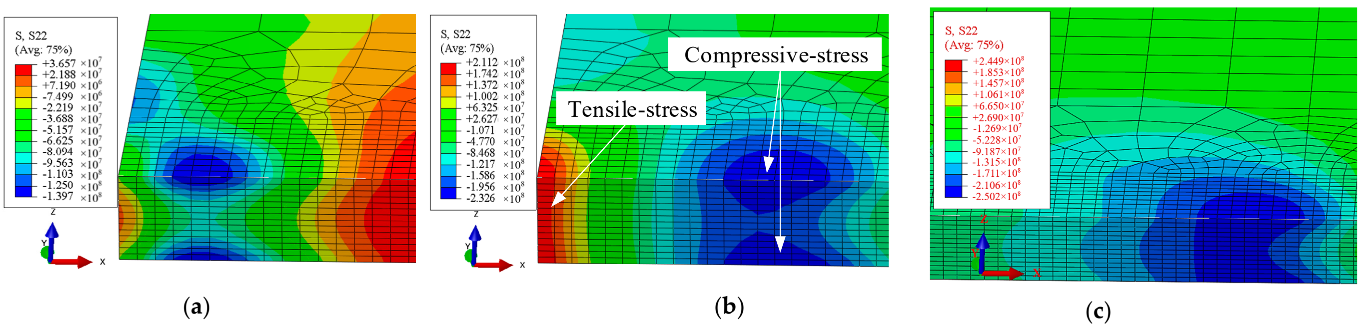

Figure 15. The distribution of transverse tensile stress in the workpiece heated by the dual-sided heat mode at (**a**) t = 0.9000 s, (**b**) t = 1.767 s and (**c**) t = 4.030 s.

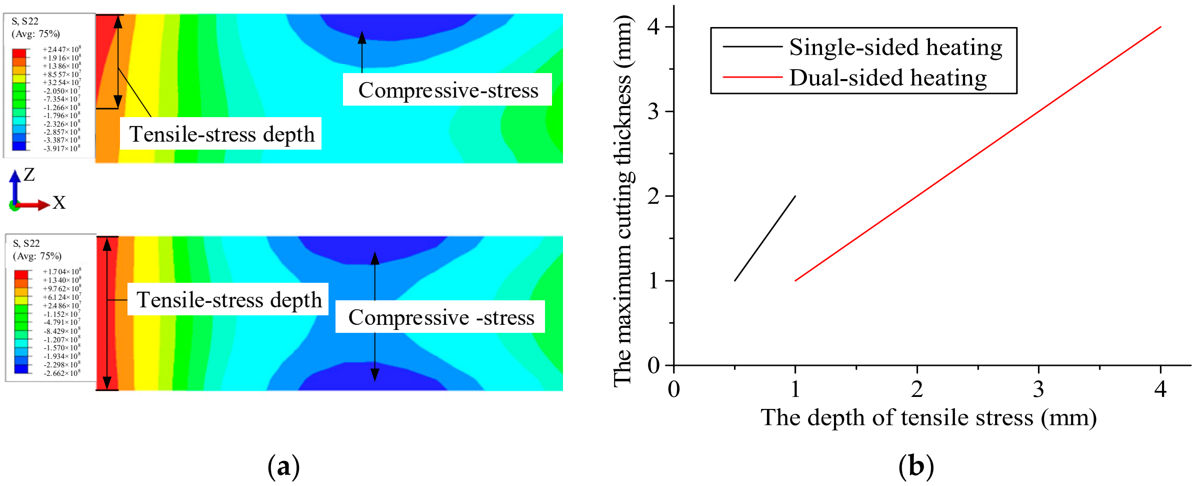

Figure 16. (**a**) Comparison of the distribution of thermal-stress between the single and dual-sided heat modes. (**b**) The effect of heat mode on the maximum cutting thickness.

4.3. Analysis of the Fracture Quality Distribution

Figure 17 shows the tensile stress evolution and crack propagation mode in the crack initiation stage in cutting Al_2O_3 ceramics using the thermal cracking method via a microwave-induced dual-sided heat source. As is shown in Figure 17a, the pre-crack first experienced the action of tensile stress as the upper and lower heat source were loaded on the edge of the workpiece.

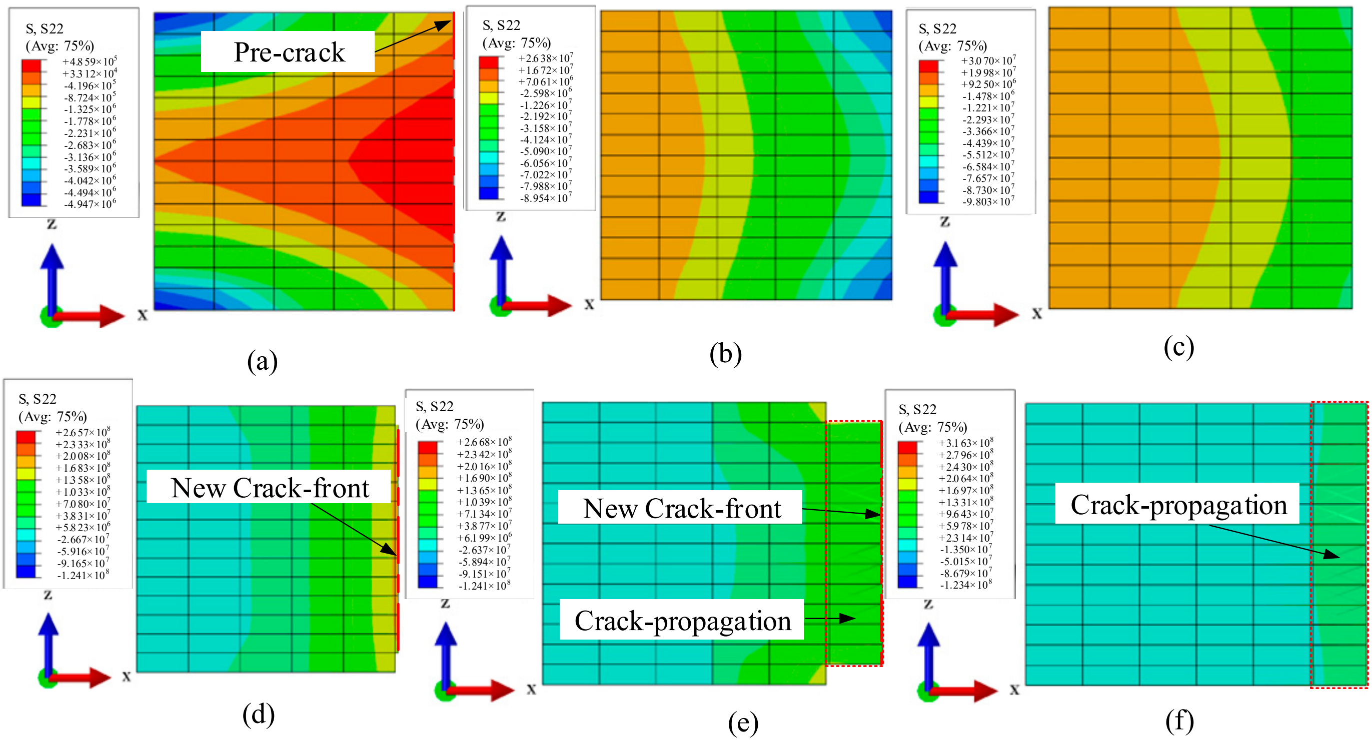

Figure 17. Transverse tensile stress evolution and initial crack behavior in cutting ceramics using thermal cracking method with microwave dual-surface heat source at (**a**) 0.06667 s, (**b**) 1.17083 s, (**c**) 1.33750 s, (**d**) 2.40857 s, (**e**) 2.42267 s and (**f**) 2.42860 s. (The microwave power is 600 W, the scanning speed is 3 mm/s, the dual-sided coated graphite thickness is 100 μm and the effective power radius 2 mm).

Then, with the dual-sided heat source moving to the site shown in Figure 17b, which was just above the pre-crack, and moving further, the tensile stress continually gathered toward the pre-crack again. At the stage shown in Figure 17d, when the tensile stress at the center thickness of the material exceeded the fracture strength, the new crack front formed. Finally, the new crack front at the center thickness propagated and drove the whole thickness to extend forward.

The initial cracking process under the action of bulk heat source was simulated to compare it with the crack initiation characteristic of dual-sided heat sources. Figure 18 shows the transverse tensile stress distribution and initial crack propagation evolution when the glass was cut by a bulk heat source. The geometric model used was the same as that used in Al_2O_3 ceramics, and the crack propagation simulation calculation was also carried out by using extended finite-element technology. The remarkable difference from the dual-sided loading mode was that the compressive stress zone, which represented the maximum temperature zone, was on the center of the material. This difference led to crack initiation near the upper and lower surface of the material, shown in Figure 18, which was also reported in Zhao's research [9].

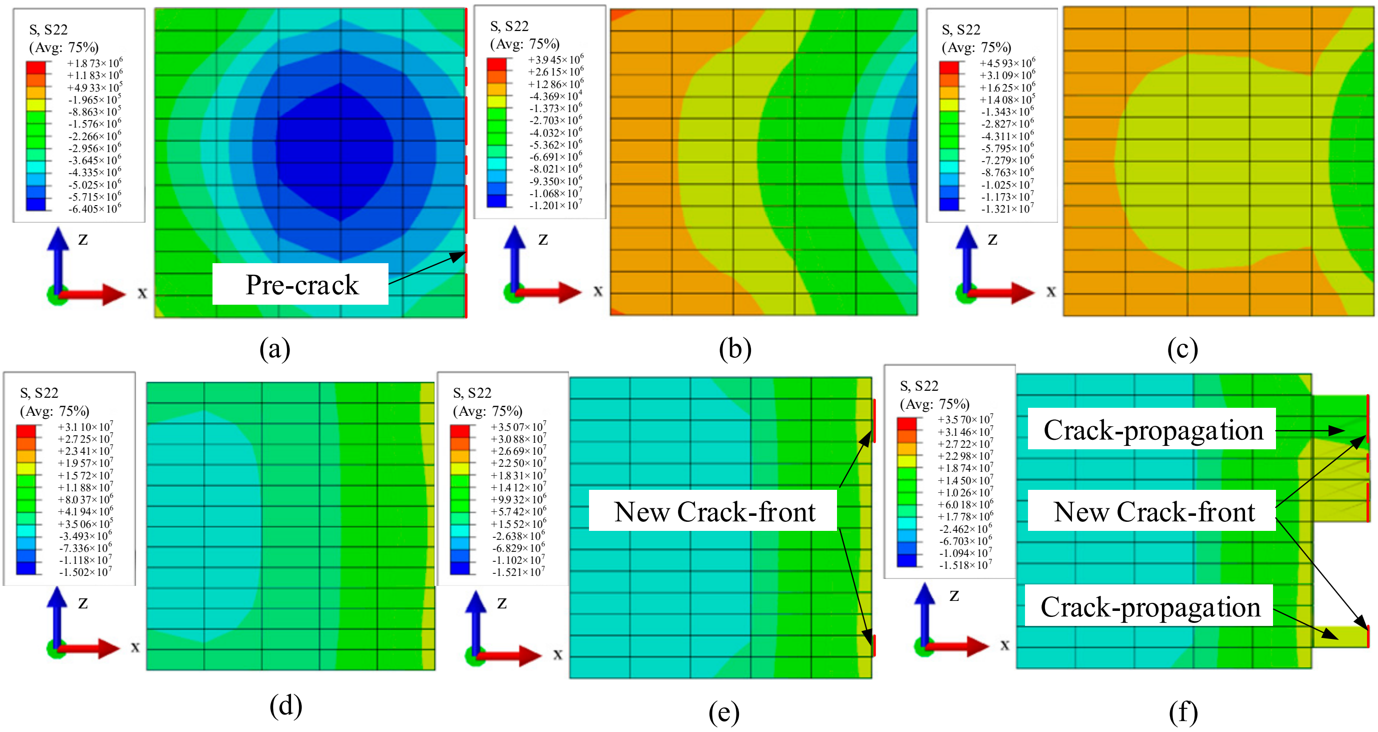

Figure 18. Transverse tensile stress evolution and crack behavior in the process of crack initiation of cutting glass using thermal cracking method via bulk heat source at (**a**) 0.8193 s, (**b**) 1.3189 s, (**c**) 1.5194 s, (**d**) 2.0206 s, (**e**) 2.1527 s and (**f**) 2.1860 s.

Figure 19 shows the transverse tensile stress distribution along the pre-crack at the time when the crack initiation occurred in the thermal cracking of ceramic materials via a dual-surface heat source (Figure 19a) and a bulk heat source (Figure 19b). From Figure 19, it can be seen that the transverse tensile stress distribution characteristic along the pre-crack in the dual-sided heat mode and the bulk heat mode was different, but together, they were more significantly different from the single-sided heat mode, which is shown in Figure 20. In the thermal cracking of glass, it was reported that the body heat mode has better cutting quality than that of the single-sided heat mode [3]. It is the similarity in the transverse tensile stress distribution style between the dual-sided heat mode and the bulk heat mode that results in their better fracture quality than the single-sided heat mode.

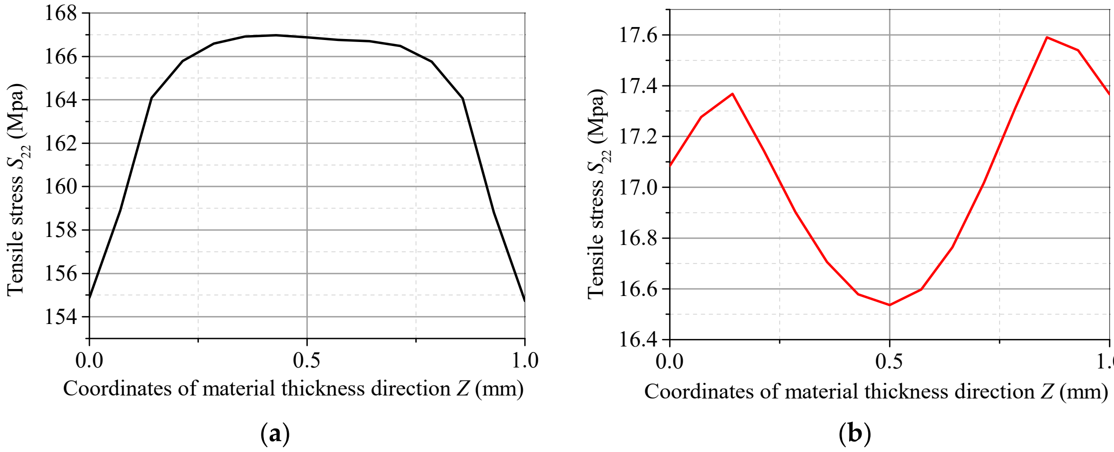

Figure 19. Transverse tensile stress distribution along crack length direction before crack initiation under the action of dual-surface heat source and comparison with that under the action of body heat source. (**a**) Dual surface heat source; (**b**) body heat source.

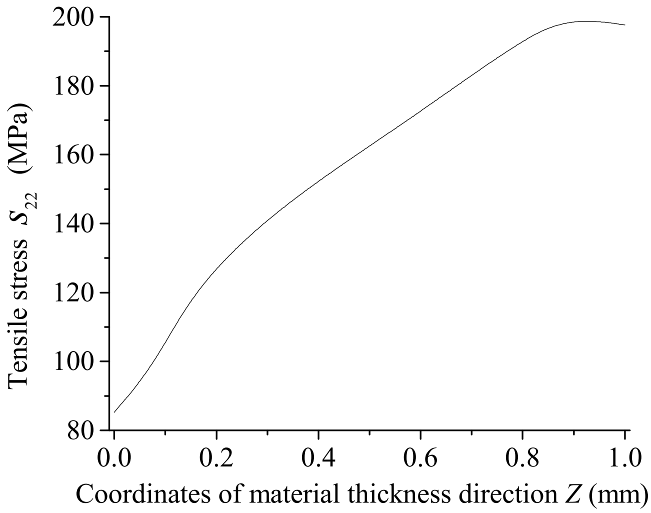

Figure 20. Transverse tensile stress distribution at the bottom of pre-crack along the direction of material thickness when the crack is expanding under single-sided heat source.

In fracture mechanics of brittle materials, a crack would propagate when the external tensile stress exceeds the fracture strength of the material. From Figure 19, it can be seen that the center thickness of the material in the dual-sided surface heat mode had approximately equal tensile stress. The workpiece would fracture first at these high-external-stress and low-gradient sections, which was accurately predicted in the crack propagation simulation in Figure 17. Because this section in the thickness had a proportion beyond 70% and this state could maintain at more than 80% of the cutting periods, the pre-crack almost synchronously propagated in a large proportion of the middle section, shown in Figure 17. Compared with the crack propagation style in the bulk heat mode, shown in Figure 18, in which the fracture first occurred near the upper and lower surface, the dual-sided surface heat mode would produce better cutting quality.

It is notable that the monotonous distribution of transverse tensile stress caused the crack to initiate from the surface with high tensile stress and then expand to another surface, shown in Figure 21, resulting in poor fracture quality and the serious uneven distribution of section quality.

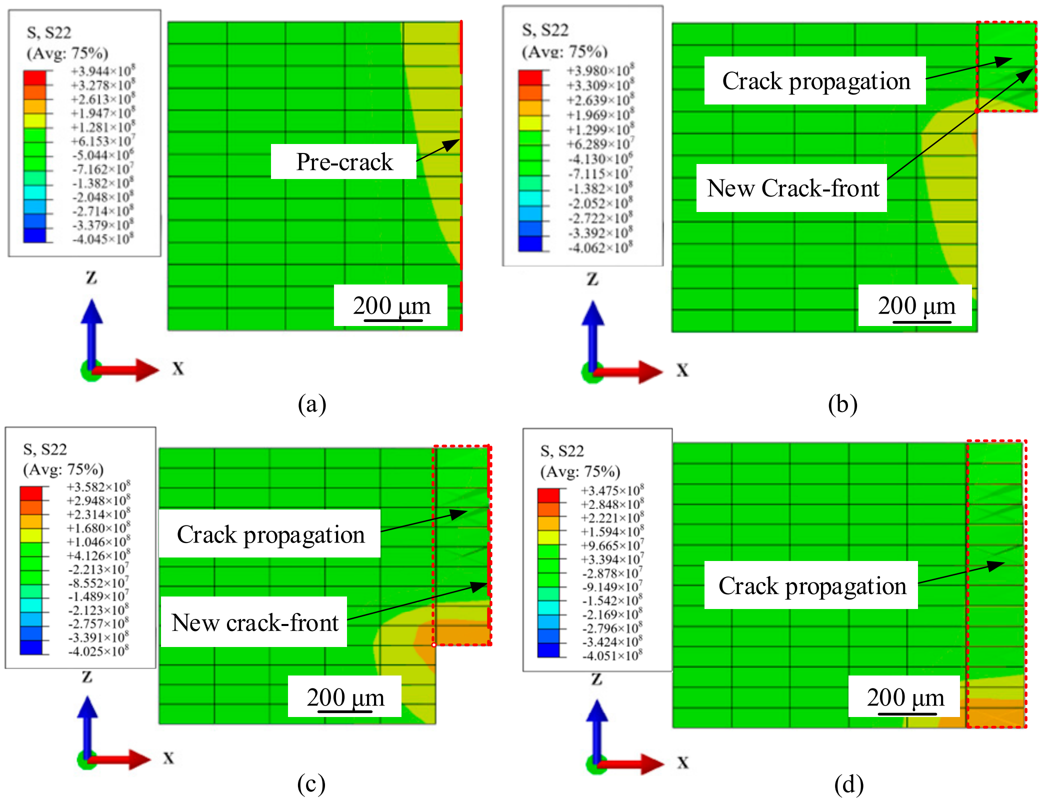

Figure 21. Crack initiation mode of Al_2O_3 ceramic under single-surface heat source at (**a**) 1.6922 s, (**b**) 1.7252 s, (**c**) 1.7269 s and (**d**) 1.7599 s.

Furthermore, it can be derived that the crack initiated at the maximum tensile stress zone. This distribution of transverse tensile stress along the thickness direction in dual-sided cutting mode is consistent with the distribution of the good section quality at the middle depth and poor section quality near the surface in the experiment. Because the more uniform stress distribution in the middle depth led to better quality in the middle depth, and the larger stress gradient near the upper and lower surfaces led to poor section quality.

5. Conclusions

In this work, the microwave-induced dual-sided thermal stress method was proposed to resolve the limited machining capacity and poor fracture quality problem produced by the single-sided heat mode in splitting opaque, brittle material using the thermal-controlled fracture method. The major conclusions from this study are summarized as follows.

The microwave-induced dual-sided thermal-cracking method was first proposed and realized. The experimental results indicate that it could improve the machining capacity by more than double compared with the single-sided mode.

The dual-sided thermal stress method provides better fracture quality and more uniform section morphology compared with the single-sided mode.

A thermal-controlled fracture model based on dual-sided thermal stress was established to calculate the temperature and the thermal stress distribution and simulate the crack propagation behavior. The simulation results had good agreement with the experiment result. The modeling was used to advance our understanding of the improvement mechanism of the machining capacity and fracture quality for this method.

The depth of the transverse tensile stress along the thickness direction of the workpiece was proven to have a positive correlation with the machining capacity by contrasting the dual-sided and single-sided thermal stress cutting method.

The reason for the better fracture quality and more uniform section morphology in the dual-sided thermal stress cutting mode is that the middle sites in the thickness direction of the workpiece could have an approximate equality transverse tensile stress zone accounting for more than 70%, and this state could be maintained in more than 80% of the cutting periods.

This study provides an innovative and feasible method for cutting opaque, brittle materials with promising fracture quality and machining capacity for industrial application. An important research direction in the future is the study of the influence of the matching of dual heat sources on stress distribution at crack fronts and its effect on machining quality.

Author Contributions: Conceptualization, Y.W. and X.C.; methodology, H.W. and Z.H.; software, X.C. and Z.H.; validation, X.C., Y.W., Z.H. and H.W.; formal analysis, X.C.; investigation, X.C.; resources, Y.W.; data curation, Z.H.; writing—original draft preparation, X.C.; writing—review and editing, X.C.; visualization, X.C.; supervision, X.C.; project administration, Y.W.; funding acquisition, X.C. All authors have read and agreed to the published version of the manuscript.

Funding: This work was supported by the Research Initiation Foundation of Anhui Polytechnic University (No. S022021002); the scientific research project of Anhui Polytechnic University (No. KZ42022065) and the Key Project of Natural Science of Anhui Provincial Department of Education (No. KJ2021A0487).

Institutional Review Board Statement: Not applicable.

Informed Consent Statement: Not applicable.

Data Availability Statement: Not applicable.

Conflicts of Interest: The authors declare no conflict of interest.

References

1. Rakshit, R.; Das, A. A review on cutting of industrial ceramic materials. *Precis. Eng.* **2019**, *59*, 90–109. [CrossRef]
2. Lumley, R.M. Controlled Separation of Brittle Materials Using a Laser. *Am. Ceram. Soc. Bull.* **1968**, *48*, 850–854.
3. Yang, L.J.; Wang, Y.; Tian, Z.G.; Cai, N. YAG laser cutting soda-lime glass with controlled fracture and volumetric heat absorption. *Int. J. Mach. Tool Manuf.* **2010**, *50*, 849–859. [CrossRef]
4. Haupt, O.; Siegel, F.; Schoonderbeek, A.; Richter, L.; Kling, R.; Ostendorf, A. Laser dicing of silicon: Comparison of ablation mechanisms with a novel technology of thermally induced stress. *J. Laser Micro Nanoeng.* **2008**, *3*, 135–140. [CrossRef]
5. Yang, L.; Ding, Y.; Cheng, B.; Mohammed, A.; Wang, Y. Numerical simulation and experimental research on reduction of taper and HAZ during laser drilling using moving focal point. *Int. J. Mach. Tool Manuf.* **2017**, *91*, 1171–1180. [CrossRef]
6. Li, C.; Piao, Y.; Meng, B.; Hu, Y.; Li, L.; Zhang, F. Phase transition and plastic deformation mechanisms induced by self-rotating grinding of GaN single crystals. *Int. J. Mach. Tool Manuf.* **2022**, *172*, 103827. [CrossRef]
7. Li, C.; Wu, Y.; Li, X.; Ma, L.; Zhang, F.; Huang, H. Deformation characteristics and surface generation modelling of crack-free grinding of GGG single crystals. *J. Mater. Process. Technol.* **2020**, *279*, 116577. [CrossRef]
8. Ueda, T.; Yamada, K.; Oiso, K.; Hosokawa, A. Thermal Stress Cleaving of Brittle Materials by Laser Beam. *Cirp. Ann.-Manuf. Technol.* **2002**, *51*, 149–152. [CrossRef]
9. Zhao, C.; Zhang, H.; Wang, Y. Semiconductor laser asymmetry cutting glass with laser induced thermal-crack propagation. *Opt. Laser Eng.* **2014**, *63*, 43–52. [CrossRef]
10. Cai, Y.; Yang, L.; Zhang, H.; Wang, Y. Laser cutting silicon-glass double layer wafer with laser induced thermal-crack propagation. *Opt. Laser Eng.* **2016**, *82*, 173–185. [CrossRef]
11. Kalyanasundaram, D.; Schmidt, A.; Molian, P.; Shrotriya, P. Hybrid CO_2 laser/waterjet machining of polycrystalline diamond substrate: Material separation through transformation induced controlled fracture. *J. Manuf. Sci. Eng.* **2014**, *136*, 1–10. [CrossRef]
12. Furumoto, T.; Hashimoto, Y.; Ogi, H.; Kawabe, T.; Yamaguchi, M.; Koyano, T.; Hosokawa, A. CO_2 laser cleavage of chemically strengthened glass. *J. Mater. Process. Technol.* **2021**, *289*, 116961. [CrossRef]
13. Liu, P.; Deng, L.; Zhang, F.; Chen, H.; Duan, J.; Zeng, X. Study on high-efficiency separation of laminated glass by skillfully combining laser-induced thermal-crack propagation and laser thermal melting. *Appl. Phys. A* **2020**, *126*, 1–13. [CrossRef]
14. Xu, J.; Hu, H.; Zhuang, C.; Ma, G.; Han, J.; Lei, Y. Controllable laser thermal cleavage of sapphire wafers. *Opt. Laser Eng.* **2018**, *102*, 26–33. [CrossRef]
15. Cheng, X.; Yang, L.; Wang, M.; Cai, Y.; Wang, Y.; Ren, Z. Laser beam induced thermal-crack propagation for asymmetric linear cutting of silicon wafer. *Opt. Laser Technol.* **2019**, *120*, 105765. [CrossRef]
16. Cheng, X.; Yang, L.; Wang, M.; Cai, Y.; Wang, Y.; Ren, Z. The unbiased propagation mechanism in laser cutting silicon wafer with laser induced thermal-crack propagation. *Appl. Phys. A* **2019**, *125*, 1–11. [CrossRef]
17. Brugan, P.; Cai, G.; Akarapu, R.; Segall, A.E. Controlled-fracture of prescored alumina ceramics using simultaneous CO_2 lasers. *J. Laser Appl.* **2006**, *18*, 236–241. [CrossRef]

18. Saman, A.M.; Furumoto, T. Evaluation of Separating Process for Different Materials by Thermal Stress Cleaving Technique. *Int. J. Precis. Eng.* **2018**, *7*, 158–161. [CrossRef]
19. Tsai, C.; Chen, H. Laser cutting of thick ceramic substrates by controlled fracture technique. *J. Mater. Process. Technol.* **2003**, *136*, 166–173. [CrossRef]
20. Wang, H.; Zhang, H.; Wang, Y. Splitting of glass and SiC ceramic sheets using controlled fracture technique with elliptic microwave spot. *Ceram. Int.* **2016**, *43*, 1669–1676. [CrossRef]
21. Cheng, X.; Zhao, C.; Wang, H.; Wang, Y.; Wang, Z. Mechanism of irregular crack-propagation in thermal controlled fracture of ceramics induced by microwave. *Mech. Ind.* **2020**, *21*, 610. [CrossRef]
22. Wang, H.; Zhang, H.; Wang, Y.; Wang, M. Thermal controlled fracture of Al2O3 substrate by inducing microwave discharge in graphite coat. *Ceram. Int.* **2019**, *45*, 6149–6159. [CrossRef]
23. Cai, Y.; Wang, M.; Zhang, H.; Yang, L.; Fu, X.; Wang, Y. Laser cutting sandwich structure glass–silicon–glass wafer with laser induced thermal—Crack propagation. *Opt. Laser Technol.* **2017**, *93*, 49–59. [CrossRef]
24. Yin, Y.; Gao, Y.; Yang, C. Sawing characteristics of diamond wire cutting sapphire crystal based on tool life cycle. *Ceram. Int.* **2021**, *47*, 26627–26634. [CrossRef]